International Conference on Mathematics, Computational Methods & Reactor Physics (M&C 2009)
Saratoga Springs, New York, May 3-7, 2009, on CD-ROM, American Nuclear Society, LaGrange Park, IL (2009)

A PIECEWISE LINEAR DISCONTINUOUS FINITE ELEMENT SPATIAL DISCRETIZATION OF THE TRANSPORT EQUATION IN 2D CYLINDRICAL GEOMETRY

Teresa S. Bailey
Lawrence Livermore National Laboratory
P.O. Box 808, L-312
Livermore, CA 94551
bailey42@llnl.gov

Marvin L. Adams
Texas A&M University
Department of Nuclear Engineering
College Station, TX 77843-3133
mladams@tamu.edu

Jae H. Chang
Los Alamos National Laboratory
P.O. Box 1663, MS D409
Los Alamos, NM 87544
jhchang@lanl.gov

James S. Warsa
Los Alamos National Laboratory
P.O. Box 1663, MS D409
Los Alamos, NM 87544
warsa@lanl.gov

ABSTRACT

We present a new spatial discretization of the discrete-ordinates transport equation in two-dimensional cylindrical (RZ) geometry for arbitrary polygonal meshes. This discretization is a discontinuous finite element method that utilizes the piecewise linear basis functions developed by Stone and Adams. We describe an asymptotic analysis that shows this method to be accurate for many problems in the thick diffusion limit on arbitrary polygons, allowing this method to be applied to radiative transfer problems with these types of meshes. We also present numerical results for multiple problems on quadrilateral grids and compare these results to the well-known bi-linear discontinuous finite element method. We conclude that the piecewise linear method extends the excellent performance of linear discontinuous (on triangles) and bilinear discontinuous (on quadrilaterals) to general polygons. This includes "polygons" generated by adding "hanging nodes" to simpler cells, via local refinement, or by "cutting" simpler cells to represent materials interfaces.

1. INTRODUCTION

Accurate solutions of radiative transfer problems require accurate solutions of the linear Boltzmann transport equation. When a deterministic approach is followed, discontinuous finite

element methods (DFEM) are often used as spatial discretizations. Using an asymptotic analysis, Adams [1] has developed requirements for DFEM weight and basis functions to produce accurate discretizations for optically thick, highly scattering regions in problems described by Cartesian coordinates. This physical regime, often called the thick diffusion limit, is highly relevant to many radiative transfer problems. In this paper, we apply the Piecewise Linear Discontinuous Finite Element (PWLD) spatial discretization, first developed by Stone and Adams [2, 3] for 2D Cartesian (XY) geometry, to the 2D cylindrical (RZ) transport equation. Using Adams's analysis we show that the PWLD method is accurate in the diffusion limit on arbitrary polygonal grids for RZ geometry. Previously, only Upstream Corner Balance [4], a DFEM based upon Wachspress's rational basis functions [5], and the Continuous Finite Element-Based, Discontinuous Finite Element Method [6] have been shown to be accurate in the diffusion limit for arbitrary polygonal cells. We test the PWLD method in RZ geometry and compare against theoretical predictions and against the Bi-linear Discontinuous Finite Element (BLD) method on a variety of problems with quadrilateral spatial cells. PWLD results agree with predictions and are very close to BLD results. We also discuss the behavior of PWLD for "poor" cells such as re-entrant cells and cells with internal angles of 180 degrees. We conclude that PWLD is an excellent candidate for RZ problems with all manner of polygonal cells, including cells with "hanging nodes" arising from local mesh refinement as well as distorted cells arising from Lagrangian hydrodynamics.

2. DERIVATION OF THE PWLD METHOD IN RZ GEOMETRY

We begin our derivation of the PWLD method in RZ geometry with a brief description of the angular differencing we applied to the RZ equation. We then derive a general DFEM discretization of the angularly differenced RZ equations for polygonal grids. We finish the description of the method by defining the PWL basis functions, and conclude this section with a discussion about "lumping" the RZ discretization.

2.1 Angular discretization applied to the RZ transport equation

The time-independent, monoenergetic discrete-ordinates RZ transport equation with isotropic scattering in conservation form is

$$\frac{\mu_{m,n}}{r}\frac{\partial}{\partial r}\left[r\psi_{m,n}(r,z)\right]-\frac{1}{r}\left[\frac{\partial}{\partial\omega}\eta\psi\right]_{m,n}+\xi_n\frac{\partial}{\partial z}\psi_{m,n}(r,z) +\sigma\psi_{m,n}(r,z)=\frac{\sigma_s}{4\pi}\phi(r,z)+\frac{1}{4\pi}S(r,z), \quad (1)$$

where ψ is the unknown angular intensity, σ is the macroscopic total cross section, σ_s is the macroscopic scattering cross section, $\mu = \vec{e}_r \bullet \vec{\Omega} = \cos\omega$ = radial component of particle direction, $\xi = \vec{e}_z \bullet \vec{\Omega}$ = axial component of particle direction, $\eta = \sin\omega$, ϕ is the scalar flux, and S is a fixed source. The m,n subscripts indicate a level-based quadrature set in which n is a level of quadrature directions with constant ξ, and m denotes a quadrature point on that level. We

difference the angular derivative term in Eq. (1) using the method described by Lewis and Miller [7].

$$\begin{aligned}\frac{\mu_{m,n}}{r}\frac{\partial}{\partial r}\left[r\psi_{m,n}\left(r,z\right)\right]+\frac{\alpha^{n}_{m+1/2}\psi_{m+1/2,n}\left(r,z\right)-\alpha^{n}_{m-1/2}\psi_{m-1/2,n}\left(r,z\right)}{rw_{m,n}}+\xi_{n}\frac{\partial}{\partial z}\psi_{m,n}\left(r,z\right)\\ +\sigma\psi_{m,n}\left(r,z\right)=\frac{\sigma_{s}}{4\pi}\phi\left(r,z\right)+\frac{1}{4\pi}S\left(r,z\right)\end{aligned}, \tag{2}$$

where

$$\begin{aligned}\alpha^{n}_{m+1/2}&=\alpha^{n}_{m-1/2}-\mu_{m,n}w_{m,n}\\ \alpha^{n}_{1/2}&=\alpha^{n}_{M_{n}+1/2}=0\end{aligned}. \tag{3}$$

The value of $\psi_{1/2,n}$ is found using a starting-direction equation, which is an XY transport equation along the $\mu=-\left(1-\xi_{n}\right)^{1/2}$ and ξ_n direction. This starting direction equation is

$$\begin{aligned}-\left(1-\xi_{n}\right)^{1/2}\frac{\partial}{\partial r}\psi_{1/2,n}\left(r,z\right)+\xi_{n}\frac{\partial}{\partial z}\psi_{1/2,n}\left(r,z\right)+\sigma\left(r,z\right)\psi_{1/2,n}\left(r,z\right)\\ =\frac{\sigma_{s}}{4\pi}\phi\left(r,z\right)+\frac{1}{4\pi}S\left(r,z\right)\end{aligned}. \tag{4}$$

To close the system, we use the weighted diamond relationship developed by Morel and Montry [8]:

$$\psi_{m,n}=\tau_{m,n}\psi_{m+1/2,n}+\left(1-\tau_{m,n}\right)\psi_{m-1/2,n}\ , \tag{5}$$

where the values of τ linearly interpolate the values of μ on each level. Eqs. (2), (4), and (5) define a system of M_n+1 equations and M_n+1 unknowns on each level in the quadrature set, where M_n is the number of quadrature directions on level n.

2.1 General DFEM discretization

The application of a discontinuous finite element method to the angularly discretized equations is straightforward and described in detail in multiple references [1,2,3,5,6,9,10]. We must apply the spatial discretization to both the regular and starting direction equations, Eqs. (2) and (4), respectively. A few simple steps are required to derive the DFEM spatial discretization.

1. Divide the spatial domain into domain-filling, non-overlapping cells.
2. Multiply the angularly discretized equations by a weight function, and integrate over a spatial cell.
3. Apply Gauss's Divergence Theorem to the integrals of the gradient term, resulting in a surface integral and a volume integral. Allow the surface intensity to differ from the cell-interior intensity evaluated at the surface. We apply the theorem a second time to the

resultant volume integral, which produces a surface integral involving a difference of surface and interior intensities and a volume integral of the gradient of the intensity.

4. Expand spatially dependent variables in terms of a set of basis functions, u_j:

$$\begin{aligned}\psi_{m,n}(\vec{r}) &= \sum_{j=1}^{J}\psi_{m,n,j}u_j(\vec{r})\\ \phi(\vec{r}) &= \sum_{j=1}^{J}\phi_j u_j(\vec{r})\\ S(\vec{r}) &= \sum_{j=1}^{J}S_j u_j(\vec{r})\end{aligned} \tag{6}$$

5. Define each surface intensity to be the intensity from the upstream cell or boundary condition.

This produces a single-cell matrix that determines the unknowns in each cell in terms of its source and its incident intensities (from upstream cells or boundary conditions). The size of this matrix is *JxJ* where *J* is the number of basis functions used to approximate the flux in the cell. The i^{th} row of a single-cell matrix is given by:

$$\begin{aligned}&\oint_{\partial A_{cell}} ds v_i \vec{n}\bullet\vec{\Omega}_{m,n} r\left\{\left(\sum_{j=1}^{J}\tilde{\psi}_{m,n,j}u_j(\vec{r})\right)-\left(\sum_{j=1}^{J}\psi_{m,n,j}u_j(\vec{r})\right)\right\}+\int_{A_{cell}} dA v_i\vec{\Omega}_{m,n}\bullet\vec{\nabla}\left[r\left(\sum_{j=1}^{J}\psi_{m,n,j}u_j(\vec{r})\right)\right]\\ &\qquad+\int_{A_{cell}} dA v_i\left[\Gamma_{m+1/2}\left(\sum_{j=1}^{J}\psi_{m,n,j}u_j(\vec{r})\right)+\sigma r\left(\sum_{j=1}^{J}\psi_{m,n,j}u_j(\vec{r})\right)\right]\\ &=\frac{1}{4\pi}\int_{A_{cell}} dA v_i\left\{r\left(\sigma_s\sum_{j=1}^{J}\phi_j u_j(\vec{r})+\sum_{j=1}^{J}S_j u_j(\vec{r})\right)+\Gamma_{m-1/2}\sum_{j=1}^{J}\psi_{m-1/2,n,j}u_j(\vec{r})\right\}\end{aligned}, \tag{7}$$

where the Γ terms are coefficients generated by the differencing of the angular derivative term, $\psi_{m,n,j}$ is the angular flux inside the cell, $\tilde{\psi}_{m,n,j}$ is the angular flux on the cell surface, ϕ_j is the scalar flux inside the cell, S_j is the source coefficient if we interpolate the source with the basis functions, v_i is the i^{th} weight function, and u_j is the j^{th} basis function. We have assumed that the cross sections are constant inside a spatial cell. The DFEM form of the corresponding starting-direction equation is

$$\begin{aligned}&\oint_{\partial A_{cell}} ds v_i \vec{n}\bullet\vec{\Omega}_{1/2,n}\left\{\left(\sum_{j=1}^{J}\tilde{\psi}_{1/2,n,j}u_j(\vec{r})\right)-\left(\sum_{j=1}^{J}\psi_{1/2,n,j}u_j(\vec{r})\right)\right\}\\ &+\int_{A_{cell}} dA v_i\vec{\Omega}_{1/2,n}\bullet\vec{\nabla}\left[\left(\sum_{j=1}^{J}\psi_{1/2,n,j}u_j(\vec{r})\right)\right]+\int_{A_{cell}} dA v_i\sigma\left(\sum_{j=1}^{J}\psi_{1/2,n,j}u_j(\vec{r})\right).\\ &=\frac{1}{4\pi}\int_{A_{cell}} dA v_i\left(\sigma_s\sum_{j=1}^{J}\phi_j u_j(\vec{r})+\sum_{j=1}^{J}S_j u_j(\vec{r})\right)\end{aligned} \tag{8}$$

The angular flux on the surface of the cell is the upwind value:

$$\tilde{\psi}_{m,n,j} = \begin{cases} \psi_{m,n,j,cell} \ \ if \ \ \vec{n} \bullet \vec{\Omega}_{m,n} > 0 \\ \psi_{m,n,upwind\ cell}\left(r,z\right)_j \ \ if \ \ \vec{n} \bullet \vec{\Omega}_{m,n} < 0 \end{cases}. \tag{9}$$

For the remainder of this paper we assume a Galerkin DFEM, which means that the i^{th} weight function is the same as the i^{th} basis function. We note that Eqs. (7) - (9) are general, holding for any set of basis functions and cell shapes.

2.2 The PWL basis functions

The PWL basis functions were originally developed by Stone and Adams [2,3] for XY spatial discretizations on arbitrary polygons. To build these functions, we divide each polygonal cell into subcells called sides. A side, shown in Figure 1, is a triangle defined by a cell center point and two adjacent vertices.

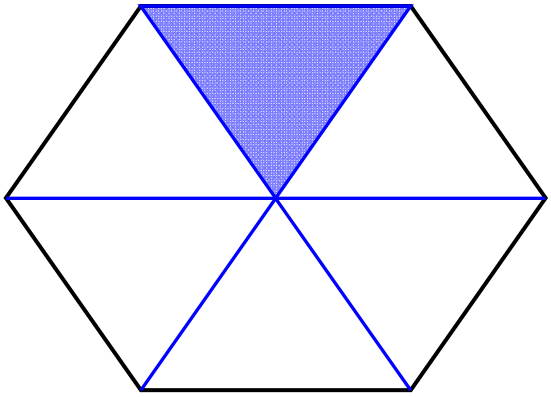

Figure 1: The shaded triangle represents a side in a hexagonal cell.

Mathematically, the PWL basis functions are defined as

$$u_i\left(r,z\right) = t_i\left(r,z\right) + \beta_i t_c\left(r,z\right), \tag{10}$$

where the t functions are standard linear functions on triangles. The support point for t_i is the i^{th} vertex and the support point for t_c is the cell center. The β_i value is a weighting parameter for the t_c contributions, and is defined such that

$$\vec{r}_c \equiv \text{ cell midpoint } = \sum_{i=1}^{N} \beta_i \vec{r}_i \ . \tag{11}$$

All calculations presented in this paper use a value of

$$\beta_i = \frac{1}{N}, \tag{12}$$

where N is the number of sides in the cell. A PWL basis function is shown in Figure 2.

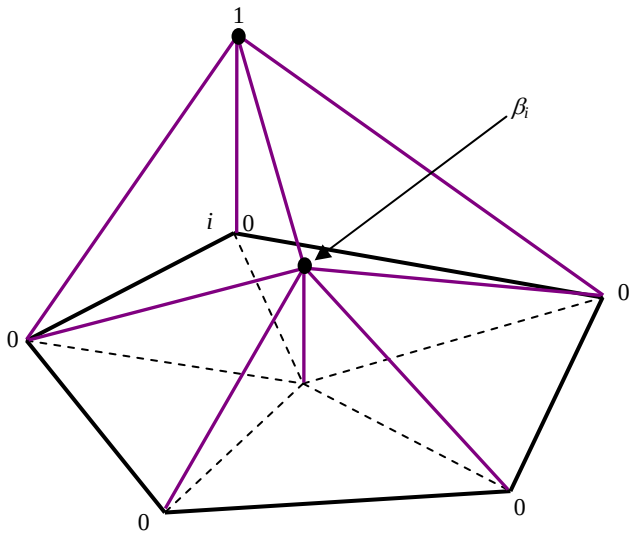

Figure 2: A PWL basis function for support point *i* on an arbitrary polygon

When the PWL basis functions are applied to Eqs. (7) and (8) they are easily integrated by dividing the integrals into sums of integrals over sides, causing the integrals in these equations to become

$$\begin{aligned} \oint_{\partial A_{cell}} ds &\longrightarrow \sum_{\substack{e=edges \\ \in cell}} \int_e ds \\ \int_{A_{cell}} dA &\longrightarrow \sum_{\substack{s=sides \\ \in cell}} \int_s dA \end{aligned} \tag{13}$$

On triangles, the PWL basis functions collapse to the same basis functions used in the Linear Discontinuous Finite Element Method (LD). As a result, the PWLD method is exactly the same as the LD method for triangular grids.

DFEMs are often “lumped” to improve robustness (resistance to oscillations, discontinuities, and negative solutions). Any integral in Eqs. (7) and (8) can be lumped by

$$\int_{\chi} d\chi v_i(\chi) \sum_{j=1}^{J} \psi_j u_j(\chi) \xrightarrow{lump} \psi_i \int_{\chi} d\chi v_i(\chi), \tag{14}$$

which makes the resultant system of equations more diagonally dominant. For RZ geometry we explore two choices for lumping the system. In the "surface-mass" lumping scheme we lump the surface, collision, and source terms. The second scheme, a "generalized lumping" scheme designed by Morel and Warsa [11] specifically for RZ, also lumps the angular-derivative term in a careful way that does not destroy desirable solution properties.

3. ASYMPTOTIC DIFFUSION LIMIT ANALYSIS

We have performed an asymptotic diffusion limit analysis for interior and boundary cells on the RZ PWLD spatial discretization of the transport equation [9]. This analysis is based on previous DFEM asymptotic analyses [1,10,12,13]. The analysis begins by scaling the physical parameters in Eqs. (7) and (8) such that the problem becomes optically thick and diffusive as the small parameter, ε, tends to zero.

$$\begin{aligned} \sigma &\to \frac{\sigma}{\varepsilon} \\ \sigma_s &\to \frac{\sigma}{\varepsilon} - \varepsilon\sigma_a \\ S &\to \varepsilon S \end{aligned} \tag{15}$$

We guess that the fluxes in these equations can be expanded in a power series in ε,

$$\begin{aligned} \psi &= \psi^{(0)} + \varepsilon\psi^{(1)} + \varepsilon^2\psi^{(2)} \ldots \\ \phi &= \phi^{(0)} + \varepsilon\phi^{(1)} + \varepsilon^2\phi^{(2)} \ldots \end{aligned}. \tag{16}$$

We then collect and equate like order terms to determine the behavior of the flux in the thick diffusion limit. In this limit, the analytic transport equation results in a leading-order scalar flux that is isotropic and described by the diffusion equation. For this reason, a method is accurate in the diffusion limit if its discretized leading-order scalar flux is isotropic and satisfies an accurate discretized form of the correct diffusion equation with accurate boundary conditions. In the interest of brevity, we will only summarize the important results of this analysis in this paper.

For interior cells, from the *O(1/ε)* terms we find that the leading-order angular flux is isotropic in both the regular and starting direction equations.

$$\psi^{(0)}_{m,n,j} = \psi^{(0)}_{1/2,n,j} = \psi^{(0)}_{m+1/2,n,j} = \frac{1}{4\pi}\phi^{(0)}_j, \text{ all } m \text{ and } n. \tag{17}$$

Then, by taking the zeroth angular moment of the *O(1)* terms, we find that the leading-order flux requires more than just surface integral terms to fully determine it. Furthermore, if lumping is applied to the surface integral terms, we find that the leading-order fluxes are pointwise continuous in the diffusion limit. A Fick's law relationship which equates the leading-order

scalar flux to the first-order current at vertex *i* in spatial cell *k* is found from the first angular moment of the *O(1)* terms. If lumping is applied to the mass matrix this is:

$$\vec{J}_{ik}^{(1)} = -D_k \sum_{j=1}^{J} \frac{\left[\sum_{\substack{\text{sides in} \\ \text{cell } k}} \left(\int_{side} dAu_i \frac{\partial\left(ru_j\right)}{\partial r} - \int_{side} dAu_i u_j \right) \hat{e}_r + \left(\frac{\partial\left(ru_j\right)}{\partial z} \int_{side} dAu_i \right) \hat{e}_z \right] \phi_{j,k}^{(0)}}{\sum_{\substack{\text{sides in} \\ \text{cell } k}} \int_{side} dVu_i}, \tag{18}$$

where

$$\begin{aligned} D_k &= \frac{1}{3\sigma_k} \\ \vec{J}_{ik} &= \sum_{n=1}^{N} \sum_{m}^{M_n} w_{m,n} \vec{\Omega}_{m,n} \psi_{m,n,i} \end{aligned} . \tag{19}$$

(Without mass-matrix lumping this relation involves the inverse of the mass matrix.) Finally, we take the zeroth angular moment of the *O(ε)* terms. We sum *O(ε)* equations for all cells surrounding vertex *i*, resulting in

$$\begin{aligned} &\sum_{\substack{k=\text{cells} \\ \text{around } i}} \left(\left(\sum_{j=1}^{J} J_{j,k,r}^{(1)} \sum_{\substack{\text{sides} \\ \in \text{cell } k}} \int_{side} dAu_{i,k} \frac{\partial\left(ru_{j,k}\right)}{\partial r} \right) - J_{i,k,r}^{(1)} \sum_{\substack{e_k = \\ \text{edges} \\ \text{with } i}} \left(n_{r,e,k} \int_e ds r u_{i,k} \right) \right) \\ &+ \sum_{\substack{k=\text{cells} \\ \text{around } i}} \left(\left(\sum_{j=1}^{J} J_{j,k,z}^{(1)} \sum_{\substack{\text{sides} \\ \in \text{cell } k}} \int_{side} dAu_{i,k} \frac{\partial\left(ru_{j,k}\right)}{\partial z} \right) - J_{i,k,z}^{(1)} \sum_{\substack{e_k = \\ \text{edges} \\ \text{with } i}} \left(n_{z,e,k} \int_e ds r u_{i,k} \right) \right). \\ &+ \sum_{\substack{k=\text{cells} \\ \text{around } i}} \sigma_{a,k} \sum_{\substack{\text{sides} \\ \in \text{cell } k}} \int_{side} dAru_{i,k} \sum_{j=1}^{J} \phi_{j,k}^{(0)} u_{j,k} = \sum_{\substack{k=\text{cells} \\ \text{around } i}} \sum_{\substack{\text{sides} \\ \in \text{cell } k}} \int_{side} dAru_{i,k} \sum_{j=1}^{J} S_{j,k}^{(0)} u_{j,k} \end{aligned} \tag{20}$$

Note that the current, *J*, in Eq. (20) has been decomposed into its *r* and *z* vector components. The coupled system of Eqs. (18) and (20) represent the i^{th} row of the coefficient matrix of the resultant discretization of the RZ diffusion equation that describes the leading-order scalar flux when vertex *i* is in the interior of the problem.

On a logically rectangular grid, the diffusion discretization results in a nine-point stencil. This diffusion discretization is not symmetric positive definite (SPD) if matrices other than the collision matrix are lumped. If we chose not to lump the surface terms, the resultant diffusion discretization would be SPD, but the leading-order scalar flux would not be pointwise continuous. It is important to note that the analysis performed for the RZ PWLD method assumed an arbitrary polygonal grid.

We also performed the asymptotic diffusion limit analysis for boundary cells, which resulted in behavior similar to other DFEMs [1]. If we assume that the incident partial current is spatially continuous, the leading-order flux on the boundary will be pointwise continuous for surface-lumped methods. Furthermore, the leading-order boundary condition for our DFEM has normal and tangential components. The normal component of this boundary condition accurately approximates the analytic leading-order boundary condition. However, the tangential component can act as a contamination term in the interior of the problem. For orthogonal cells, the tangential component of the boundary condition does not contaminate the interior solutions. For non-orthogonal cells, errors from the tangential component can propagate into the interior of the problem. This troubling tangential term in the boundary condition appears for all DFEMs. A significant amount of work is still required to quantify the effect of non-orthogonal boundary cells on the accuracy of DFEMs in the diffusion limit. The boundary cell analysis was also performed for an arbitrary polygonal grid, although not all of the special-case results are discussed here [4, 9].

4. NUMERICAL TEST PROBLEMS

We implemented the PWLD discretization for the RZ transport equation in Capsaicin, a transport code being developed at Los Alamos National Laboratory. To test the effectiveness of the method, we examine the truncation error of the PWLD method compared with the BLD method on a variety of problems. Truncation error test problems are used to determine the order by which the solution of the numerical method converges to the actual solution. This order is *n* if the error in the solution decreases by a factor of to 2^n every time the mesh is refined by a factor of two in each dimension.

The first truncation error problem has a manufactured solution,

$$\phi(r,z) = \left[\sin(\pi r) + 1 - r\right]\sin(\pi z). \tag{21}$$

We used a level symmetric quadrature set for this test problem. We first tested the unlumped version of PWLD on both rectangular and randomized quadrilateral meshes. Figure 3 shows the truncation error of PWLD and BLD on these meshes. The reference line in this figure and all subsequent truncation error figures is an arbitrary line with a slope representative of second-order convergence behavior. The behavior and magnitude of the error for both unlumped methods is almost identical, and the error between the two meshes is extremely close. Furthermore, both methods exhibit second-order convergence behavior, which is expected.

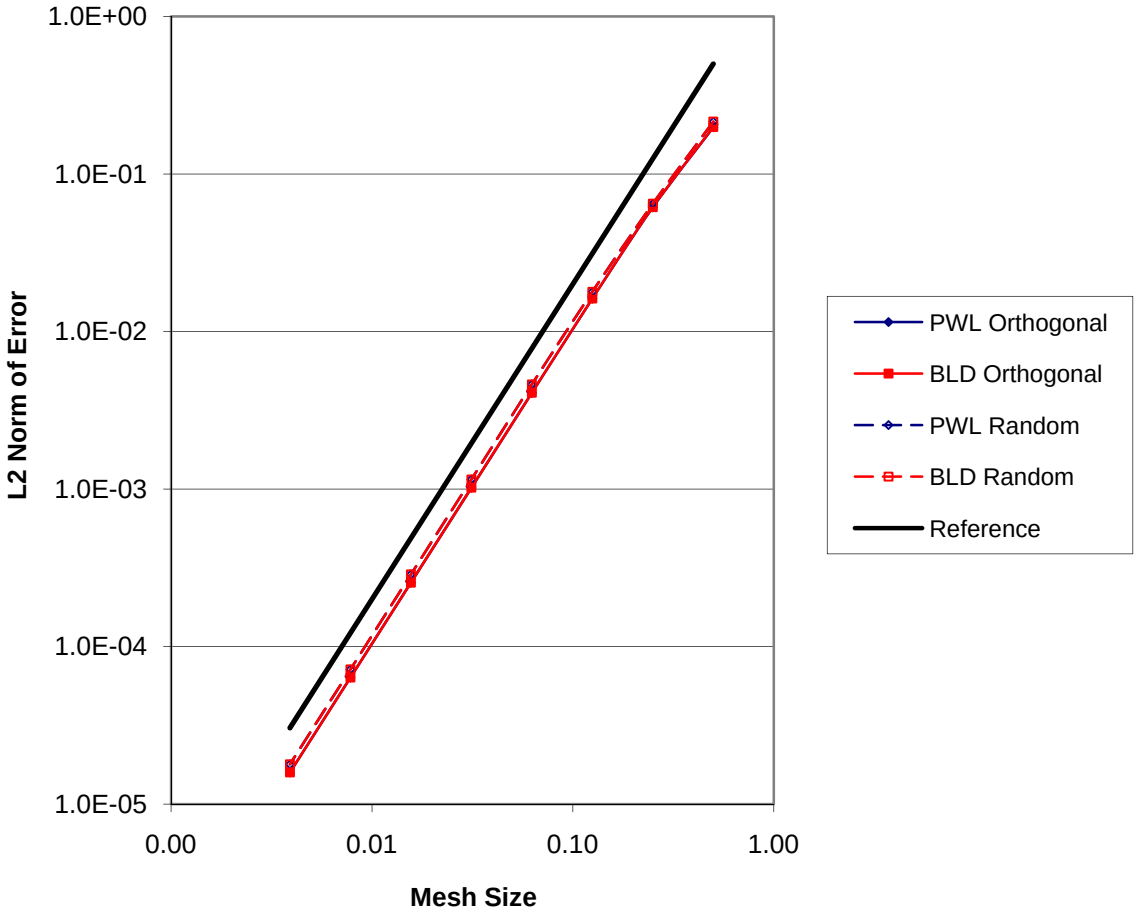

Figure 3: Truncation error of unlumped methods

We then tested both the surface-mass lumped and the generalized lumped versions of PWLD and BLD on the orthogonal and random meshes. The results of these test problems are shown in Figure 4. This plot shows that, for this test problem, the type of lumping makes no difference in the solution. These results also suggest that the lumped solutions on random grids are slightly less accurate than lumped solutions on orthogonal grids. Comparison of the two figures shows that for this problem (whose solution is very smooth), the L_2 errors of the lumped methods are smaller than those of the unlumped methods.

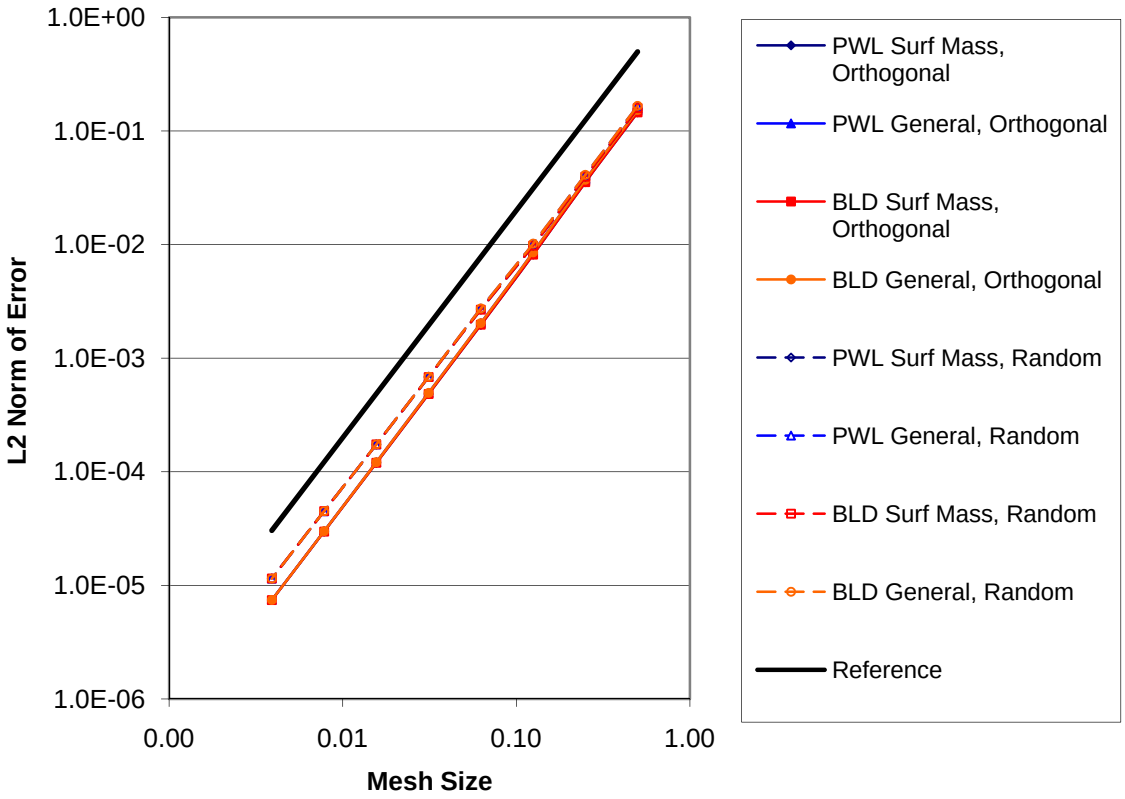

Figure 4: Truncation error of lumped methods

We also studied the truncation error of the lumped methods for a diffusive problem, in which the cells are small relative to diffusion lengths, but large relative to mean free paths. This problem was developed by Morel and Warsa to test their generalized lumping scheme [11]. It is a one-dimensional problem that has an analytic solution of

$$\phi(z) = \frac{S}{D}\left\{\left[\frac{1-e^{1/L}}{e^{-1/L}-e^{1/L}}-1\right]e^{z/L}+\left[\frac{e^{1/L}-1}{e^{-1/L}-e^{1/L}}\right]e^{-z/L}+1\right\}+O\left(\varepsilon^2\right) \qquad (22)$$

$$\varepsilon \approx \frac{1}{\sqrt{1-c}} \approx 10^{-3}$$

with a total cross section of 8192 cm^{-1} and a scattering ratio of 0.9999987. L in Eq. (22) is the diffusion length, $1/[\sigma_t\,(3(1-c))^{1/2}]$. We ran this problem on a randomized quadrilateral mesh of N cells in the z direction and $N/4$ cells in the r direction, and used an S_8 product Gauss-Chebyshev quadrature set. The results of this truncation error problem, shown in Figure 5, indicate that lumped PWLD has almost identical accuracy as lumped BLD in the thick diffusive limit, and

that all methods exhibit second-order convergence behavior. These results also indicate that the two PWLD lumping methods have nearly identical convergence properties for this problem.

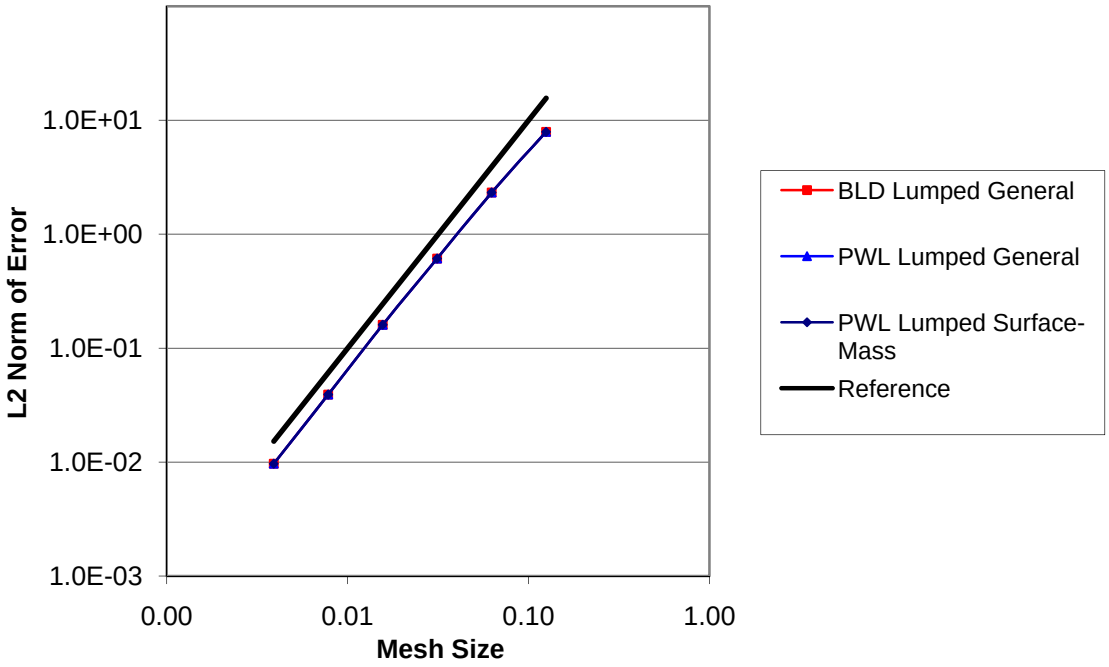

Figure 5: Truncation Error of lumped methods on diffusive test problem

This problem not only reinforces the results of our diffusion limit analysis, it also underscores the simplicity of adding the PWLD method to a mature code that contains the BLD method. In Capsaicin, we were able to use for PWLD the Diffusion Synthetic Acceleration (DSA) scheme that was implemented for BLD. Recently it has been shown that using DSA as a preconditioner for a GMRES iterative solution can produce rapid and robust convergence even without a "consistent" diffusion discretization [14,15]. Our successful use of the existing diffusion discretization in Capsaicin adds further evidence to this effect. This is also partly due to PWL's close relationship to BLD and its similar robustness and accuracy.

5. DISCUSSION

Given that PWLD is identical to LD on triangles and provides almost the same results as BLD on quadrilaterals, it is fair to ask what motivation exists to use it instead of LD or BLD. We are motivated by flexibility that it offers in the spatial grids used for transport solutions and by the simplicity of having a single method that handles every grid types. When PWLD is coded for general polygons, as it is in our codes, it can provide accurate solutions given grids with any combination of the following kinds of cells:

- Polygons with any number of sides;

- Triangles with "hanging nodes," as from local mesh refinement (treated as quadrilaterals with 180-degree corners);
- Quadrilaterals with hanging nodes, as from local mesh refinement (treated as pentagons with 180-degree corners);
- Re-entrant polygons, for example arising from Lagrangian hydrodynamics;
- "Cut" cells formed by dividing standard cells into two or more polygons to accurately represent material interfaces.

Testing and analysis indicate that the method performs well even with interior angles that reach and exceed 180 degrees [9]. Thus, while standard grid generators may never routinely generate polygons with more than four sides, we see significant practical value in being able to handle the cases described above as well as all combinations of them.

6. CONCLUSIONS

The results from the asymptotic diffusion limit analysis and the numerical test problems indicate that the PWLD method is an excellent candidate for discretizing the two-dimensional (RZ) transport equation. In the thick diffusion limit the leading-order PWLD solution satisfies an accurate diffusion discretization, as desired. This remains true in the presence of unresolved boundary layers, although PWLD shares with other DFEMs the property that distorted boundary cells can cause some boundary layers to introduce errors into the leading-order solution. Our preliminary test problems show that the PWLD method is as accurate as the BLD method on problems in the thin and diffusion limits. PWLD is identical to LD on triangles and provides essentially the same solution as BLD on quadrilaterals, but is easily applied to higher polygons (whereas LD and BLD fail on such polygons in diffusive problems). We see significant utility in the ability to directly treat polygonal cells, including hanging-node cells that arise from local mesh refinement as well as "cut cells" obtained, for example, by dividing rectangular cells to represent non-orthogonal interfaces.

ACKNOWLEDGMENTS

This work was partially funded by the Computational Science Graduate Fellowship. This work performed under the auspices of the U.S. Department of Energy by Lawrence Livermore National Laboratory under Contract DE-AC52-07NA27344.

REFERENCES

1. M. L. Adams, "Discontinuous Finite Element Transport Solutions in Thick Diffusive Problems," *Nucl. Sci. and Eng.* **137**, 298-333 (2001).
2. H. G. Stone and M. L. Adams, "A Piecewise Linear Finite Element Basis with Application to Particle Transport," *Proc. ANS Topical Meeting Nuclear Mathematical and Computational Sciences Meeting*, Gatlinburg, TN, April 6-11, 2003, CD-ROM (2003).
3. H. G. Stone and M.L. Adams, "New Spatial Discretization Methods for Transport on Unstructured Grids," *Proc. ANS Topical Meeting Mathematics and Computation, Supercomputing, Reactor Physics and Biological Applications*, Avignon, France, September 12-15, 2005, CD-ROM (2005).

4. M. L. Adams, “Subcell Balance Methods for Radiative Transfer on Arbitrary Grids,” *Transport Theory Statist. Phys.* **26**, 385-431, (1997).
5. G. G. Davidson and T. S. Palmer, “Finite Element Transport Using Wachspress Rational Basis Functions on Quadrilaterals in Diffusive Regions,” *Nucl. Sci. and Eng.* **159**, 242-255 (2008).
6. J. S. Warsa, “A Continuous Finite Element-Based, Discontinuous Finite Element Method for S_N Transport,” *Nucl. Sci. and Eng.* **160**, 385-400 (2008).
7. E. E. Lewis and W. F. Miller, *Computational Methods of Neutron Transport*, American Nuclear Society, La Grange Park, Il (1993).
8. J. E. Morel and G. R. Montry, “Analysis and Elimination of the Discrete-Ordinates Flux Dip,” *Transport Theory Statis. Phys.* **13**, 615-633, (1984).
9. T. S. Bailey, “The Piecewise Linear Discontinuous Finite Element Method Applied to the RZ and XYZ Transport Equations,” Doctoral Dissertation, Texas A&M University (2008).
10. T. S. Palmer, “Curvilinear Geometry Transport Discretizations in Thick Diffusive Regions,” Doctoral Dissertation, University of Michigan (1993).
11. J. E. Morel and J. S. Warsa, “A Lumped Bi-Linear Discontinuous S_n Spatial Discretization for RZ Quadrilateral Meshes,” *Trans. Am. Nucl. Soc.*, **95**, 873-875 (2006).
12. E. W. Larsen, J. E. Morel, and W. F. Miller, “Asymptotic Solutions of Numerical Transport Problems in Optically Thick, Diffusive Regimes,” *J. Comput. Phys.* **69**, 283-324 (1987).
13. T. S. Palmer and M. L. Adams, “Curvilinear Geometry Transport Discretizations in the ‘Thick’ Diffusion Limit,” *Proc. Int. Conf. Mathematical methods and Supercomputing in Nuclear Applications*, Karlsrühe, Germany, April 19-23, 1993, Vol. I, p. 3, Kernforschungszentrum, Karlsrühe (1993).
14. J. S. Warsa, T. A. Wareing, and J. E. Morel, “Fully Consistent Diffusion Synthetic Acceleration of Linear Discontinuous S_N Transport Discretizations on Unstructured Tetrahedral Meshes,” *Nucl. Sci. and Eng.* **141**, 236-251 (2002).
15. J. S. Warsa, T. A. Wareing, and J. E. Morel, “Krylov Iterative Methods and the Degraded Effectiveness of Diffusion Synthetic Acceleration for Multidimensional S_N Calculations in Problems with Material Discontinuities,” *Nucl. Sci. and Eng.* **147**, 218-248 (2004).